

REFERENCE COPY

WHEN FINISHED WITH THIS DOCUMENT
CALL

c.2

SANDIA REPORT

SAND90-1249 • UC-427
Unlimited Release
Printed June 1990

Gridless Electrostatic Field Solver for Particle Simulation Codes in Cylindrical Geometry

I. R. Shokair, J. S. Wagner

Prepared by
Sandia National Laboratories
Albuquerque, New Mexico 87185 and Livermore, California 94550
for the United States Department of Energy
under Contract DE-AC04-76DP00789



SAND90-1249
0002
UNCLASSIFIED

06/90
30P STAC

Issued by Sandia National Laboratories, operated for the United States Department of Energy by Sandia Corporation.

NOTICE: This report was prepared as an account of work sponsored by an agency of the United States Government. Neither the United States Government nor any agency thereof, nor any of their employees, nor any of their contractors, subcontractors, or their employees, makes any warranty, express or implied, or assumes any legal liability or responsibility for the accuracy, completeness, or usefulness of any information, apparatus, product, or process disclosed, or represents that its use would not infringe privately owned rights. Reference herein to any specific commercial product, process, or service by trade name, trademark, manufacturer, or otherwise, does not necessarily constitute or imply its endorsement, recommendation, or favoring by the United States Government, any agency thereof or any of their contractors or subcontractors. The views and opinions expressed herein do not necessarily state or reflect those of the United States Government, any agency thereof or any of their contractors.

Printed in the United States of America. This report has been reproduced directly from the best available copy.

Available to DOE and DOE contractors from
Office of Scientific and Technical Information
PO Box 62
Oak Ridge, TN 37831

Prices available from (615) 576-8401, FTS 626-8401

Available to the public from
National Technical Information Service
US Department of Commerce
5285 Port Royal Rd
Springfield, VA 22161

NTIS price codes
Printed copy: A03
Microfiche copy: A01

SAND90-1249
Unlimited Release
Printed June 1990

**GRIDLESS ELECTROSTATIC FIELD SOLVER FOR PARTICLE
SIMULATION CODES IN CYLINDRICAL GEOMETRY**

I. R. Shokair and J. S. Wagner
Sandia National Laboratories
Plasma Theory Division
P. O. Box 5800
Albuquerque, New Mexico 87185

ABSTRACT

A new gridless electrostatic field solver which utilizes Fourier decomposition in the azimuthal coordinate has been developed and tested. The scaling with the number of simulation particles is $N \log N$. This algorithm has been implemented in the BUCKSHOT code, which originally used a direct summation algorithm with N^2 scaling. The Fourier decomposition in the new algorithm is done about the center of mass of each species, thus nonlinear ion hose physics is included in the $m = 0$ mode. Higher order modes describe non-axisymmetric profile changes. The breakeven point between the new solver and the direct summation algorithm is about $N = 64$ particles per species when up to $m = 2$ Fourier modes are kept. For a typical ion hose simulation with 256 particles per species the new solver is faster by a factor of about 2.7.

I. Introduction

Relativistic electron beams propagating in the ion focused regime (IFR) undergo transverse (betatron) oscillations which result in an instability called the ion hose instability.⁽¹⁾ Because of the small ratio of the transverse energy to the longitudinal energy, it is customary to invoke the paraxial approximation and then decouple the transverse and longitudinal motions, using $v_z \approx c$ in the transverse equations where v_z is the axial velocity and c is the speed of light. In IFR propagation, the main interactions are those caused by the beam and ion channel space charge and the beam self magnetic field. These interactions are governed by Poisson's equation.

In general, the beam and channel can have arbitrary density profiles with strongly anharmonic potentials. Also, the ion hose instability results in strong azimuthal asymmetries in the profiles. In these types of potentials the particle orbits are very complex and thus because of these difficulties, one of the most effective methods of analyzing the physics of relativistic electron beam propagation in the IFR is via computer simulations.

Since the betatron wavelength for relativistic electron beams in the IFR is usually much larger than the amplitude of the transverse oscillations and the beam and channel transverse dimensions, the beam and channel can be divided into segments, where within each segment, the transverse interaction can be represented to a good approximation by infinitely long filaments of charge and current with no interaction between filaments in different segments.⁽²⁾ Within each segment, the fields on a filament (also referred to as particle) can be calculated using Poisson's equation and then the equations of motion can be solved and the particles pushed for the next step. A particle simulation code that makes use of the above approximations is the BUCKSHOT code.⁽³⁻⁴⁾ In this code the field on a particle is found by direct summation over all the other particles within a segment. Thus no grid is used. This makes the code very simple and suitable for use in IFR propagation problems with no physical boundary. The disadvantage of the code, however, is that the cpu time scales as N^2 where N is the number of simulation particles in a segment. Other gridless Poisson field solvers have been developed such as the Fast Multipole Expansion algorithm⁽⁵⁾ which scale with $N \log N$, however, the breakeven point between this kind of an algorithm and the direct summation is usually for an unacceptably large number of particles on vector machines such as the CRAY X-MP supercomputer.

In this report we consider an alternate approach to the solution of Poisson's equation in 2-D for a many particle system without utilizing a grid. This approach is based on Fourier decomposition in the azimuthal direction and writing the electric field in terms of radial integrals which are then replaced by sums over the particles. The overall scaling with the number of particles is $N \log N$ as will be described in the following sections. Asymptotically the algorithm also scales linearly with M , the number of Fourier modes kept in the expansion. However, for IFR propagation problems for which this algorithm was developed we find that low values of M (typically 2-4) are sufficient to resolve the azimuthal dependence. This is the case because the Fourier decomposition is done about the the center of mass of each charged particle species. This will be described in detail later.

In the next few sections we describe in detail the theory for this solver. In section II we derive the solution of Poisson's equation for a general charge distribution in 2-D cylindrical geometry. In section III this solution is applied to a system of point

particles and the algorithm for the field solver is developed. The extension to finite sized particles is made in section IV, where a specific charge distribution is chosen for the simulation particles in order to keep the $N \log N$ scaling. In the last section, the algorithm is implemented in the BUCKSHOT code and a comparison between the direct summation solver and this new solver is made for an IFR propagation problem with strong ion hose growth. The CPU time for the two solvers is also compared for different numbers of particles.

II. Solution of Poisson's Equation in Cylindrical Geometry

The situation of interest is to solve Poisson's equation in two dimensional cylindrical geometry (r, θ) for an unbounded and arbitrary charge distribution. For this situation, Poisson's equation is:

$$\frac{1}{r} \frac{\partial}{\partial r} \left(r \frac{\partial \phi}{\partial r} \right) + \frac{1}{r^2} \frac{\partial^2 \phi}{\partial \theta^2} = -4\pi\rho \quad (1)$$

where ϕ is the potential and ρ is the charge distribution. The boundary conditions on Eq. (1) are that ϕ is finite at $r = 0$ and goes to zero in the limit of $r \rightarrow \infty$. The functions ϕ and ρ can be written in their Fourier series representations as:

$$\phi(r, \theta) = \sum_{m=-\infty}^{\infty} \phi_m(r) e^{im\theta} \quad (2)$$

$$\rho(r, \theta) = \sum_{m=-\infty}^{\infty} \rho_m(r) e^{im\theta} \quad (3)$$

The resulting equations for ϕ_m and ρ_m are:

$$\rho_m(r) = \frac{1}{2\pi} \int_0^{2\pi} d\theta e^{-im\theta} \rho(r, \theta) \quad (4)$$

$$\frac{1}{r} \frac{\partial}{\partial r} \left(r \frac{\partial \phi_m}{\partial r} \right) - \frac{m^2}{r^2} \phi_m(r) = -4\pi\rho_m \quad (5)$$

Equation (5) can be solved using a Green's function, which can be found easily as:

$$G_m(r; r') = \left\{ \begin{array}{ll} \frac{-1}{2|m|} \left(\frac{r_{<}}{r_{>}} \right)^{|m|} & m \neq 0 \\ \ln(r_{>}) & m = 0 \end{array} \right\} \quad (6)$$

where $r_{<} = \min(r, r')$ and $r_{>} = \max(r, r')$.

The general solution to Eq. (5) is:

$$\phi_m(r) = -4\pi \int_0^\infty dr' r' \rho_m(r') G_m(r; r') \quad (7)$$

or

$$\phi_0(r) = -4\pi \left[\int_0^r dr' r' \rho_0(r') \ln(r) + \int_r^\infty dr' r' \rho_0(r') \ln(r') \right] \quad (8)$$

$$\phi_m(r) = \frac{4\pi}{2|m|} \left[\int_0^r dr' r' \rho_m(r') \left(\frac{r'}{r}\right)^{|m|} + \int_r^\infty dr' r' \rho_m(r') \left(\frac{r}{r'}\right)^{|m|} \right]$$

The radial and azimuthal electric field components can be obtained using $\mathbf{E} = -\nabla\phi$:

$$E_r(r, \theta) = -\frac{\partial\phi}{\partial r} = -\sum_{m=1}^{\infty} \left(\frac{\partial\phi_m}{\partial r} e^{im\theta} + \frac{\partial\phi_{-m}}{\partial r} e^{-im\theta} \right) - \frac{\partial\phi_0}{\partial r} \quad (9)$$

$$E_\theta(r, \theta) = -\frac{1}{r} \frac{\partial\phi}{\partial\theta} = -\sum_{m=1}^{\infty} \frac{im}{r} \left(\phi_m e^{im\theta} - \phi_{-m} e^{-im\theta} \right)$$

Using Eq. (8) in Eq. (9), we can obtain the following expressions for the electric field components:

$$E_r(r, \theta) = \frac{2}{r} \int_0^{2\pi} d\theta' \int_0^r dr' r' \rho(r', \theta') + \frac{2}{r} \sum_{m=1}^{\infty} \int_0^{2\pi} d\theta' \cos [m(\theta - \theta')] . \quad (10)$$

$$\left\{ \int_0^r dr' r' \left(\frac{r'}{r}\right)^m \rho(r', \theta') - \int_r^\infty dr' r' \left(\frac{r}{r'}\right)^m \rho(r', \theta') \right\}$$

$$E_\theta(r, \theta) = \frac{2}{r} \sum_{m=1}^{\infty} \int_0^{2\pi} d\theta' \sin [m(\theta - \theta')] . \quad (11)$$

$$\left\{ \int_0^r dr' r' \left(\frac{r'}{r}\right)^m \rho(r', \theta') + \int_r^\infty dr' r' \left(\frac{r}{r'}\right)^m \rho(r', \theta') \right\}$$

III. Solution for Point Particles

If in a simulation the charges are represented by point particles, then the charge density can be written as:

$$\rho(r, \theta) = \sum_{i=1}^N q_i \delta_r(r - r_i) \delta(\theta - \theta_i) \quad (12)$$

where q_i is the charge of the i 'th particle, r_i, θ_i denote the position of the particle and the δ -functions are defined such that

$$\int_0^{\infty} dr' r' \delta_r(r - r') = 1 ; \quad \int_0^{2\pi} d\theta' \delta(\theta - \theta') = 1$$

Let us assume that the particles are sorted in ascending order so that

$r_1 < r_2 < \dots < r_i < r_{i+1} < \dots < r_N$. The fields at a point r, θ with $r_n < r < r_{n+1}$ are given by:

$$E_r(r, \theta) = \frac{2}{r} \sum_{i=1}^n q_i + \frac{2}{r} \sum_{m=1}^{\infty} \left[\sum_{i=1}^n q_i \cos [m(\theta - \theta_i)] \left(\frac{r_i}{r}\right)^m - \sum_{i=n+1}^N q_i \cos [m(\theta - \theta_i)] \left(\frac{r}{r_i}\right)^m \right] \quad (13)$$

$$E_{\theta}(r, \theta) = \frac{2}{r} \sum_{m=1}^{\infty} \left[\sum_{i=1}^n q_i \sin [m(\theta - \theta_i)] \left(\frac{r_i}{r}\right)^m + \sum_{i=n+1}^N q_i \sin [m(\theta - \theta_i)] \left(\frac{r}{r_i}\right)^m \right] \quad (14)$$

Define the sums:

$$S_0(n) = \sum_{i=1}^n q_i$$

$$S_1^m(n) = \sum_{i=1}^n q_i r_i^m \sin m\theta_i$$

$$S_2^m(n) = \sum_{i=1}^n q_i r_i^m \cos m\theta_i \quad (15)$$

$$S_3^m(n) = \sum_{i=n+1}^N q_i \frac{1}{r_i^m} \sin m\theta_i$$

$$S_4^m(n) = \sum_{i=n+1}^N q_i \frac{1}{r_i^m} \cos m\theta_i$$

In terms of these sums the fields in Eqs. (13-14) become:

$$E_r(r, \theta) = \frac{2}{r} S_0(n) + \frac{2}{r} \sum_{m=1}^{\infty} \left[\frac{1}{r^m} (\cos m\theta S_2^m(n) + \sin m\theta S_1^m(n)) - r^m (\cos m\theta S_4^m(n) + \sin m\theta S_3^m(n)) \right] \quad (16)$$

$$E_{\theta}(r, \theta) = \frac{2}{r} \sum_{m=1}^{\infty} \left[\frac{1}{r^m} (\sin m\theta S_2^m(n) - \cos m\theta S_1^m(n)) + r^m (\sin m\theta S_4^m(n) - \cos m\theta S_3^m(n)) \right] \quad (17)$$

In the numerical evaluation of Eqs. (16-17), the Fourier series is truncated at a value of $m = M$, where M is sufficient to resolve the azimuthal structure of the problem under consideration. Typically in a particle simulation code the fields need to be evaluated at the particle positions in order to solve the equations of motion for the particles. Thus, evaluation of Eqs. (16-17) is a process that scales with N . The evaluation of the sums in Eq. (15) is also a process that scales with N . In general the particle radii need to be sorted in ascending order, which is a process that scales with $N \log N$.⁽⁶⁾ Thus the overall scaling of an algorithm based on the above method is $N \log N$, N being the number of simulation particles.

In Fig. (1) we show a plot of the radial electric field for a charge distribution made up of 256 point particles loaded with a Gaussian distribution and for $M = 2$. This field is compared to the field from a true Gaussian distribution,

$$E(r) = \frac{2I}{cr} (1 - e^{-r^2/a^2})$$

where $I = ecN$ is an effective current with N being the density per unit length and a is the Gaussian radius. In Fig. (2) we plot the actual simulation particle positions. The singularities in the field for near particle interactions are replaced by discontinuities. This is due to the truncation of the Fourier series at a small value of M . The near field singularities are recoverable if the number of Fourier modes kept in the expansion approaches the number of simulation particles. As will be discussed in the last section, the field discontinuities due to point particles cause non-physical emittance growth, unless the step size (for finite differencing) is chosen to be small enough so as to resolve the discontinuities accurately. Since the running time for a given problem is inversely proportional to the step size, a method is needed that does not require a smaller step size than that set by the physical characteristics of the problem. Such a method is the use of finite-sized particles, which is the subject of the next section.

IV. Solution with Finite-sized Particles

The use of finite-sized particles in particle simulation codes is a common technique.⁽⁷⁾ If the particle size is chosen appropriately, there should be no loss in physical phenomena and the step size should not be smaller than the physics in the problem requires. To see what is involved with finite-sized particles and how they affect a gridless algorithm, consider an axisymmetric situation where we need to evaluate a simple field integral of the form:

$$E(r) = \int_0^r dr' r' \rho(r')$$

Let the charge density be represented by the sum over discrete particles each with charge density $g(r-r_i)$, that is:

$$\rho(r) = \sum_{i=1}^N q_i g(r-r_i)$$

and

(18)

$$E(r) = \sum_{i=1}^N q_i \int_0^r dr' r' g(r' - r_i)$$

If the function $g(r'-r_i)$ is analytic and is monotonically decreasing for increasing $|r'-r_i|$, then such a function is not separable in r' and r_i , that is, the function $g(r'-r_i)$ can not be written as a product of a function of r' and another function of r_i . This immediately implies an N^2 scaling to evaluate Eq. (18) at N points. Clearly this has no advantage over the direct summation algorithm.

The simplest form for a particle density distribution that results in a separable solution is a square particle, that is:

$$g(r' - r_i) = \begin{cases} c & |r' - r_i| < a \\ 0 & |r' - r_i| > a \end{cases}$$

For this density, integrals such as in Eq. (18) result in integer powers which are clearly separable. With such a particle distribution, the discontinuities in the field are eliminated, however, $\partial E/\partial r$ will be discontinuous at the particle boundary. For continuous field derivatives of order n at the particle boundary, the particle density also needs to have continuous derivatives of order $(n-1)$ at the boundary.

In general the charge density can be written as: $\rho(r,\theta) = \sum q_i g_i(r,\theta)$. The simplest density distribution in two dimensions is of the form:

$$g_i(r,\theta) = C_i H(r - r_i, a) H(\theta - \theta_i, \Delta_i) \quad (19)$$

where the function $H(x,a)$ is unity for $|x| < a$ and zero otherwise, a is a measure of particle extent in the radial direction and Δ_i is the angular extent of the i 'th particle. The

normalization of the density requires that $C_i = 1/(4a r_i \Delta_i)$. To have reasonably square profiles we choose $\Delta_i = a/r_i$, which gives $C_i = 1/4a^2$. For particles that lie close to the origin so that $r_i - a < 0$, Eq. (19) breaks down. The simplest way to overcome this difficulty is to have position dependent particle size for those particles, such that the condition $r_i - a > 0$ is always satisfied. For large enough number of particles, this restriction does not have any impact on the physics as will be shown in the following section.

For the particle charge density given by Eq. (19), the radial and azimuthal integrals that need to be evaluated in Eqs. (10-11) are:

$$Q_1^i(r) = \int_0^r dr' r' H(r' - r_i, a) \quad Q_2^{mi}(r) = \int_0^r dr' r' \left(\frac{r'}{r}\right)^m H(r' - r_i, a)$$

$$Q_3^{mi}(r) = \int_r^\infty dr' r' \left(\frac{r}{r'}\right)^m H(r' - r_i, a)$$

$$P_1^i(\theta) = \int_0^{2\pi} d\theta' H(\theta' - \theta_i, \Delta_i) \quad P_2^{mi}(\theta) = \int_0^{2\pi} d\theta' \cos[m(\theta - \theta')] H(\theta' - \theta_i, \Delta_i)$$

$$P_3^{mi}(\theta) = \int_0^{2\pi} d\theta' \sin[m(\theta - \theta')] H(\theta' - \theta_i, \Delta_i)$$

In terms of these quantities, the radial and azimuthal fields can be written as:

$$E_r(r, \theta) = \frac{2}{r} \sum_{i=1}^N q_i C_i \left[P_1^i(\theta) Q_1^i(r) + \sum_{m=1}^{\infty} P_2^{mi}(\theta) (Q_2^{mi}(r) - Q_3^{mi}(r)) \right] \quad (21)$$

$$E_\theta(r, \theta) = \frac{2}{r} \sum_{i=1}^N q_i C_i \left[\sum_{m=1}^{\infty} P_3^{mi}(\theta) (Q_2^{mi}(r) + Q_3^{mi}(r)) \right] \quad (22)$$

The azimuthal integrals are easily evaluated and the results are:

$$P_1^i(\theta) = 2\Delta_i$$

$$P_2^{mi}(\theta) = \frac{2}{m} \cos [m(\theta - \theta_i)] \sin m\Delta_i \quad (23)$$

$$P_3^{mi}(\theta) = \frac{2}{m} \sin [m(\theta - \theta_i)] \sin m\Delta_i$$

For the radial integrals, three cases need to be distinguished based on the position of the field point relative to the particle radial position.

I. $r > r_i + a$

In this case the field point r is above the particle boundary and we have:

$$Q_1^i(r) = \frac{1}{2} \left[(r_i + a)^2 - (r_i - a)^2 \right]$$
$$Q_2^{mi}(r) = \frac{1}{(m+2) r^m} \left[(r_i + a)^{m+2} - (r_i - a)^{m+2} \right] \quad (24)$$

$$Q_3^{mi}(r) = 0$$

II. $r_i - a < r < r_i + a$

In this case the field point r overlaps with the particle and the radial integrals become:

$$Q_1^i(r) = \frac{1}{2} \left[r^2 - (r_i - a)^2 \right]$$
$$Q_2^{mi}(r) = \frac{1}{(m+2) r^m} \left[r^{m+2} - (r_i - a)^{m+2} \right] \quad (25)$$

$$Q_3^{mi}(r) = \left\{ \begin{array}{ll} \frac{r^m}{2-m} \left[(r_i + a)^{2-m} - r^{2-m} \right] & m \neq 2 \\ r^m \ln \left(\frac{r_i + a}{r} \right) & m = 2 \end{array} \right\}$$

III. $r < r_i - a$

In this case the field point r lies below the particle and the result is:

$$Q_1^i(r) = 0$$
$$Q_2^{mi}(r) = 0 \quad (26)$$

$$Q_3^{mi}(r) = \left\{ \begin{array}{ll} \frac{r^m}{2-m} \left[(r_i + a)^{2-m} - (r_i - a)^{2-m} \right] & m \neq 2 \\ r^m \ln \left(\frac{r_i + a}{r_i - a} \right) & m = 2 \end{array} \right\}$$

It is clear that all the expressions in Eqs. (21-26) are separable in r and r_i and thus scaling with the number of particles, N , is possible. Since the fields at a point r involve sums over all the particles, we can write:

$$\sum_{i=1}^N [] = \sum_{i=1}^k [] + \sum_{i=k+1}^j [] + \sum_{i=j+1}^N [] \quad (27)$$

where j and k for a given field point r are defined by:

$$\begin{aligned} r_j - a < r < r_{j+1} - a \\ r_k + a < r < r_{k+1} - a \end{aligned} \quad (28)$$

The first sum in Eq. (27) involves case I. radial integrals, the second involves case II. and the third involves case III. From Eq. (28) it is clear that if $j = k$, then no particles overlap with the field point r . For N particles which are sorted in ascending order of radii, r_1, r_2, \dots , the indices k and j for a field point r , can be found using the bisection method, which is a process that scales with $\log N$. We denote this process by the locating process.

Summary of the Fields

Having worked out the framework for the field calculations we now write down detailed expressions which can directly be used for computation purposes. Define the following expressions:

$$I_1(r, \theta) = \sum_{i=1}^N q_i C_i P_1^i(\theta) Q_1^i(r)$$

$$I_2^m(r, \theta) = \sum_{i=1}^N q_i C_i P_2^{mi}(\theta) Q_2^{mi}(r)$$

$$I_3^m(r, \theta) = \sum_{i=1}^N q_i C_i P_2^{mi}(\theta) Q_3^{mi}(r)$$

$$I_4^m(r, \theta) = \sum_{i=1}^N q_i C_i P_3^{mi}(\theta) Q_2^{mi}(r)$$

$$I_5^m(r, \theta) = \sum_{i=1}^N q_i C_i P_3^{mi}(\theta) Q_3^{mi}(r)$$

Using these expressions, the fields are:

$$E_r(r, \theta) = \frac{2}{r} \left[I_1(r, \theta) + \sum_{m=1}^{\infty} \left(I_2^m(r, \theta) - I_3^m(r, \theta) \right) \right] \quad (29)$$

$$E_\theta(r, \theta) = \frac{2}{r} \sum_{m=1}^{\infty} \left(I_4^m(r, \theta) + I_5^m(r, \theta) \right) \quad (30)$$

Define the sums:

$$S_{12}^m(k) = \sum_{i=1}^k q_i C_i (r_i + a)^{m+2} \sin m\Delta_i \begin{pmatrix} \sin m\theta_i \\ \cos m\theta_i \end{pmatrix}$$

$$S_{34}^m(k) = \sum_{i=1}^k q_i C_i \sin m\Delta_i \begin{pmatrix} \sin m\theta_i \\ \cos m\theta_i \end{pmatrix}$$

$$S_{56}^m(k) = \sum_{i=1}^k q_i C_i (r_i - a)^{m+2} \sin m\Delta_i \begin{pmatrix} \sin m\theta_i \\ \cos m\theta_i \end{pmatrix}$$

$$G_{12}^m(k) = \sum_{i=k+1}^N q_i C_i \sin m\Delta_i \begin{pmatrix} \sin m\theta_i \\ \cos m\theta_i \end{pmatrix} \begin{cases} (r_i + a)^{2-m} & m \neq 2 \\ \ln(r_i + a) & m = 2 \end{cases}$$

$$G_3^m(k) = S_3^m(k)$$

$$G_4^m(k) = S_4^m(k)$$

$$G_{56}^m(k) = \sum_{i=k+1}^N q_i C_i \sin m\Delta_i \begin{pmatrix} \sin m\theta_i \\ \cos m\theta_i \end{pmatrix} \begin{cases} (r_i - a)^{2-m} & m \neq 2 \\ \ln(r_i - a) & m = 2 \end{cases}$$

$$L_1(k) = \sum_{i=1}^k q_i C_i \Delta_i [(r_i + a)^2 - (r_i - a)^2]$$

$$L_2(k) = \sum_{i=1}^k q_i C_i \Delta_i$$

$$L_3(k) = \sum_{i=1}^k q_i C_i (r_i - a)^2 \Delta_i$$

In terms of these sums we have:

$$I_1(r, \theta) = L_1(k) + r^2 (L_2(j) - L_2(k)) - L_3(j) + L_3(k) \quad (31)$$

$$I_2^m(r, \theta) = \frac{2}{m(m+2)r^m} \left\{ \cos m\theta (S_2^m(k) - S_6^m(j)) + \sin m\theta (S_1^m(k) - S_5^m(j)) \right. \\ \left. + r^{m+2} \cos m\theta (S_4^m(j) - S_4^m(k)) + r^{m+2} \sin m\theta (S_3^m(j) - S_3^m(k)) \right\} \quad (32)$$

$$I_3^m(r, \theta) = \alpha_m r^m \left\{ \cos m\theta (G_2^m(k) - G_6^m(j)) + \sin m\theta (G_1^m(k) - G_5^m(j)) \right. \\ \left. - f_m(r) \cos m\theta (G_4^m(j) - G_4^m(k)) - f_m(r) \sin m\theta (G_3^m(j) - G_3^m(k)) \right\} \quad (33)$$

$$I_4^m(r, \theta) = \frac{2}{m(m+2)r^m} \left\{ \sin m\theta (S_2^m(k) - S_6^m(j)) - \cos m\theta (S_1^m(k) - S_5^m(j)) \right. \\ \left. + r^{m+2} \sin m\theta (S_4^m(j) - S_4^m(k)) - r^{m+2} \cos m\theta (S_3^m(j) - S_3^m(k)) \right\} \quad (34)$$

$$I_5^m(r, \theta) = \alpha_m r^m \left\{ \sin m\theta (G_2^m(k) - G_6^m(j)) - \cos m\theta (G_1^m(k) - G_5^m(j)) \right. \\ \left. - f_m(r) \sin m\theta (G_4^m(j) - G_4^m(k)) + f_m(r) \cos m\theta (G_3^m(j) - G_3^m(k)) \right\} \quad (35)$$

$$\text{where } \left\{ \begin{array}{l} \alpha_m = \frac{2}{m(2-m)}, \quad f_m(r) = r^{2-m} \quad m \neq 2 \\ \alpha_m = 1, \quad f_m(r) = \ln(r) \quad m = 2 \end{array} \right\}$$

Again the indices k and j are found by Eq. (28). The evaluation of the above sums is a process that scales with N . Since both the sorting and locating processes scale with $N \log N$ (for N particles and N field points), the overall scaling of an algorithm based on the above formalism will be $N \log N$, which is the desired scaling.

V. Application to the BUCKSHOT CODE

BUCKSHOT is a gridless particle simulation code that was written primarily for the purpose of studying the ion hose instability⁽³⁻⁴⁾, which is an electrostatic instability that develops on a relativistic electron beam propagating on an ion channel in the ion focused regime⁽¹⁾. In the code, the beam and plasma channel (ions and electrons) are divided into slices and each slice is represented by a collection of filaments with specified charge and current. The equations of motion for the filaments are solved in the plane transverse to the direction of propagation. The forces on a given filament (also referred to as particle) are due to filaments within the same slice, that is forces from adjacent slices are neglected. The beam is assumed to propagate in the axial direction at the speed of light, that is, the

paraxial approximation is invoked. Electrodynamic effects are assumed to be small for problems of interest and are not included in the code.

The equations of motion solved by the code for particles within a slice (in the case with no applied magnetic field) are:

$$\frac{\partial^2 \vec{r}_i^b}{\partial z^2} = \sum_s \frac{1}{N_s} \alpha_{bs} \sum_{j=1}^{N_s} \frac{\vec{r}_i^b - \vec{r}_j^s}{\left[\left(\vec{r}_i^b - \vec{r}_j^s \right)^2 + r_p^2 \right]}, \quad (37)$$

$$\frac{\partial^2 \vec{r}_i^c}{\partial \xi^2} = \sum_s \frac{1}{N_s} \alpha_{cs} \sum_{j=1}^{N_s} \frac{\vec{r}_i^c - \vec{r}_j^s}{\left[\left(\vec{r}_i^c - \vec{r}_j^s \right)^2 + r_p^2 \right]}, \quad (38)$$

where r_i is the position of the i 'th particle in the transverse plane, z is the axial distance and ξ is the slice variable defined by: $\xi = ct - z$, where t is the time measured in the lab frame. The superscript b denotes beam particles and c denotes channel particles (both electrons and ions). The sum over s is over all the species in the problem, N_s is the number of simulation particles for the s 'th species in the slice, r_p is the simulation particle radius and the matrix α is defined by:

$$\alpha = \frac{2eI_b}{c^3} \begin{bmatrix} 1/(\gamma^3 m_e) & -f/(\gamma m_e) & f/(\gamma m_e) \\ \frac{1}{m_i} & \frac{f}{m_i} & -\frac{f}{m_i} \\ \frac{1}{m_e} & -\frac{f}{m_e} & \frac{f}{m_e} \end{bmatrix}, \quad (39)$$

where I_b is the beam current, γ is the relativistic factor for beam electrons, f is the neutralization fraction (channel line density/beam line density), m_e is the electron rest mass and m_i is the ion mass. The additional factor of $1/\gamma^2$ in the matrix element α_{bb} results from the near cancellation of the radial electric field and azimuthal magnetic field of the beam. The force law used in Eqs. (37-38) assumes Bennett profiles of radius r_p for the simulation particles.

For a slice, the sums in Eqs. (37-38) need to be evaluated N times, where N is the total number of particles in the slice: $N = \sum N_s$, thus the execution time of the code scales as N^2 . Because of the simplicity of the algorithm and vectorization capability of CRAY computers, the code is relatively fast for a moderate number of particles (around $N = 100$). However, as N increases, the cost becomes prohibitively expensive.

The algorithm developed in the previous section was implemented in a new version of the BUCKSHOT code which gave it the desired $N \log N$ scaling and still maintained vectorization. To keep the number of Fourier modes small, the Fourier decomposition of the fields is done about the center of mass of each species. Using this technique, it is possible to simulate nonlinear ion hose physics with only the $m = 0$ mode. Typically up to $m = 2$ modes are kept in order to accommodate non-axisymmetric changes in profile shapes of the beam and channel. For problems with high order azimuthal structure, a large number of Fourier modes will be required. This might result in roundoff problems in

the evaluation of the sums as well as slowing down of the code. With these limitations we expect that this algorithm is not well suited for problems with high order ($M > 8$) azimuthal structure. In Fig. (3) we compare the cpu time (normalized) for both versions of the code which clearly shows the N^2 and $N \log N$ scalings. The breakeven point is about 64 particles/species/slice when $m = 2$ modes are kept. For a typical problem with 256 particles/species /slice, the new version is about 2.7 times faster than the old one when up to $m = 2$ modes are kept.

As was discussed earlier, it is important to choose the particle size in a simulation to be small enough so as not to wash out important physics and yet it must be large enough so that field fluctuations are small. In Fig. (4) we compare the radial electric fields for both the new and old versions of BUCKSHOT with the exact field for a Gaussian charge distribution for different particle sizes. For the old version the particles have Bennett profiles and for the new the profiles are given by Eq. (19). The same particle loading algorithm is used for both versions and it is shown in Fig. (2). In general it is found that a particle size given by: $r_p = 2 r_b / \sqrt{N}$ is sufficient to keep the field fluctuation level low enough. The effect of field fluctuations can be seen by considering single particle orbits in the charge distribution. In Fig. (5) we show such orbits for a single electron which moves axially at the speed of light c and undergoes radial oscillations according to :

$$\gamma^m_e \frac{d^2 x}{dz^2} = \frac{-eE_x(X)}{c^2}$$

where E_x is the x-field due to the charge distribution and γ is the relativistic factor for the electron. It is clear from Fig. 5c-d (only the step size is different) that when the step size is large compared to the scale length of variation of the field fluctuations, these fluctuations are not resolved and numerically the potential seems time varying or nonconservative. This is why the amplitude varies in Fig. 5c when the particle size is small and the step size is large.

The new and old solvers were compared for an IFR (Ion Focused Regime) propagation problem with the following parameters:

Beam radius	$r_b = 4.0$ cm
Ion channel radius	$r_i = 3.7$ cm
Beam offset	$x_b = 0.3$ cm
	$y_b = 0.2$ cm
Beam current	$I_b = 700$ Amps
Ion mass	$m_i = 0.28 m_p$
Relativistic factor	$\gamma = 5.9$
Axial magnetic field	$B_z = 30.0$ Gauss
Channel neutralization	$f = 1.0$
Particles/slice/species	$N = 256$
Particle radius	$r_p = 0.6$ cm
Step size	$dz = 5.0$ cm
Ion oscillation length	$\lambda_i = 970$ cm
Betatron wavelength	$\lambda_{\beta e} = 390$ cm

The beam simulation particles are loaded with a Gaussian profile with the corresponding equilibrium velocity distribution.⁽⁸⁾ The ions are loaded with a Gaussian profile at rest. The results for slice histories of the beam and channel radius and displacements are shown in Figs. (6-11) for different slices. The results using the new solver for $M = 2$ and $M = 4$ show excellent agreement, indicating that $M = 2$ is sufficient to resolve the azimuthal structure for this problem. The results using the direct summation solver agree with the new one to within 5-10% . This difference can be attributed to the different particle charge density profiles used in the two algorithms. Since the ion hose instability results in considerable changes in the beam and channel profiles, small differences in the initial fields, as seen in Fig. (4) for example, are sufficient to cause the observed 5-10% variations between the two algorithms. For the simulation with $M = 2$ the new algorithm is approximately 2.7 times faster than the direct summation algorithm.

References

1. H. L. Buchanan, Phys. Fluids, Vol. 30, 221 (1987).
2. K. A. Brueckner, Proc. Annual Propagation Phys. Rev. DARPA/SDIO/Services, 406, Monterey, CA (1985).
3. J. S. Wagner, "BUCKSHOT, a 3-D Gridless Magnetostatic Particle Code", Sandia National Laboratory Report SAND87-2019, to be published.
4. I. R. Shokair and J. S. Wagner, "Analysis and Benchmarking Calculations for the BUCKSHOT Code", Sandia National Laboratory Report SAND87-2015, November 1988.
5. L. Greengard and V. Rokhlin, J. Comp. Physics, Vol. 73, 325 (1987).
6. W. H. Press, B. P. Flannery, S. A. Teukolsky and W. T. Vetterling, Numerical Recipes, The Art of Scientific Computing, Cambridge University Press, 1986.
7. T. Tajima, Computational Plasma Physics: With Applications to Fusion and Astrophysics, Addison-Wesley Publishing Company, 1989.
8. E. P. Lee, "Velocity Distribution in a Pinched Beam", Lawrence Livermore National Laboratory Report UCID-18303, 1979.

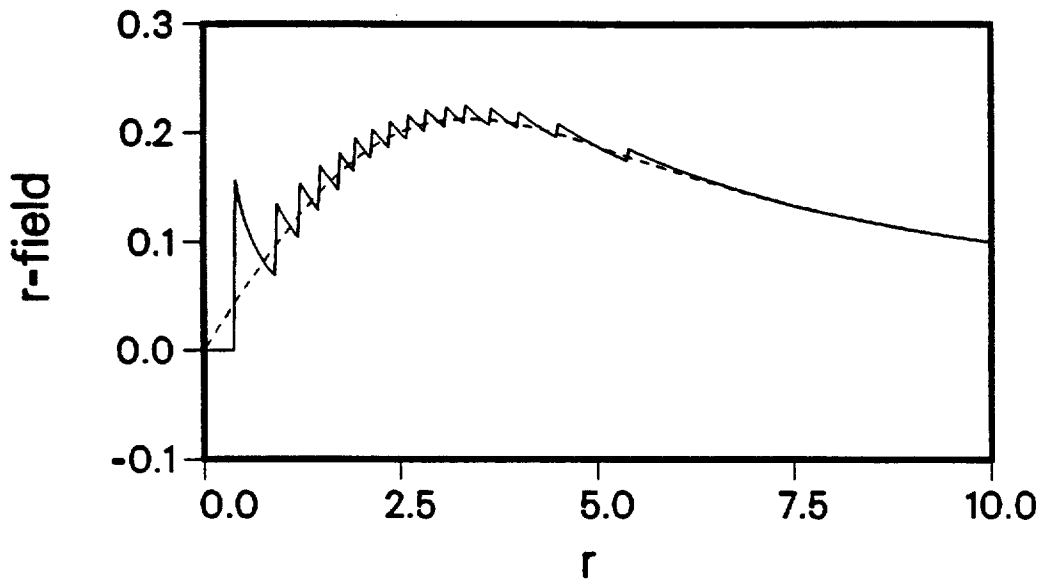


Fig. 1. Normalized radial electric field for a Gaussian charge distribution of radius $a = 3$. The solid line is field for 256 point particles with $M = 2$. The dashed line is the exact field.

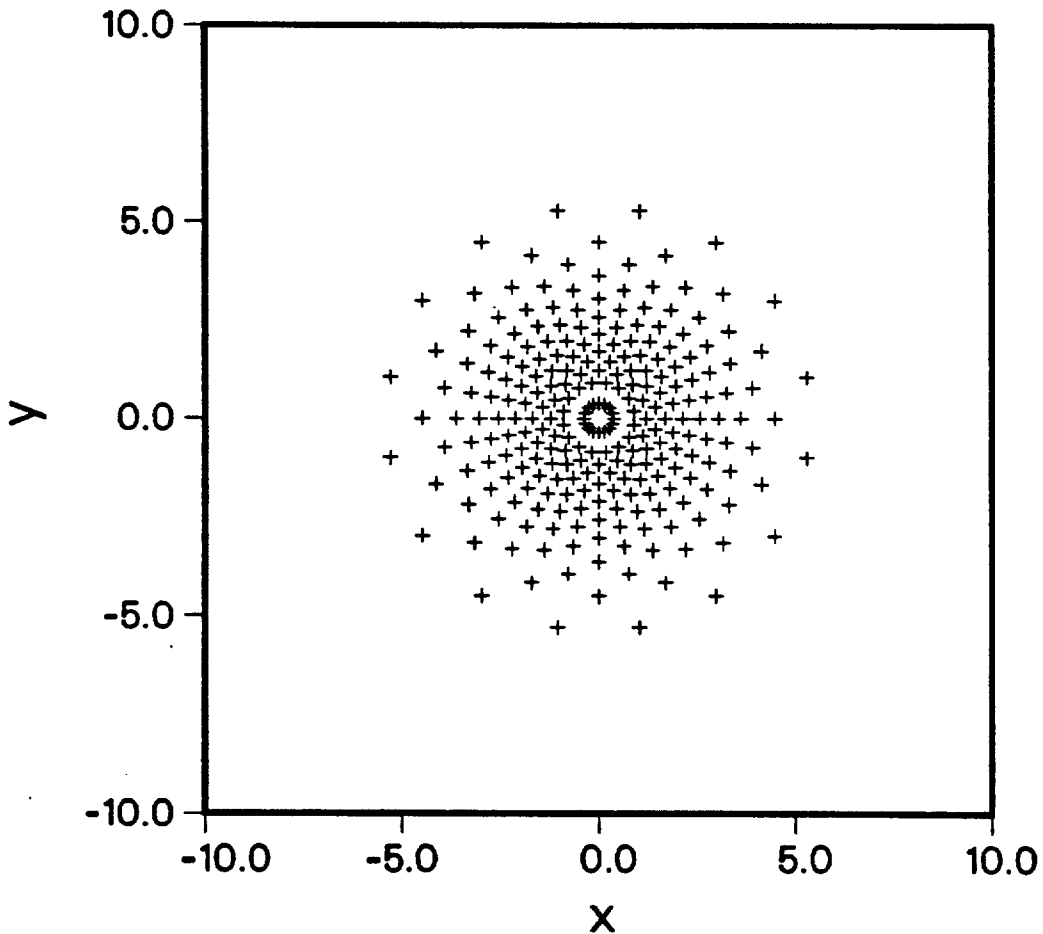


Fig. 2. Positions of simulation particles for a Gaussian distribution.

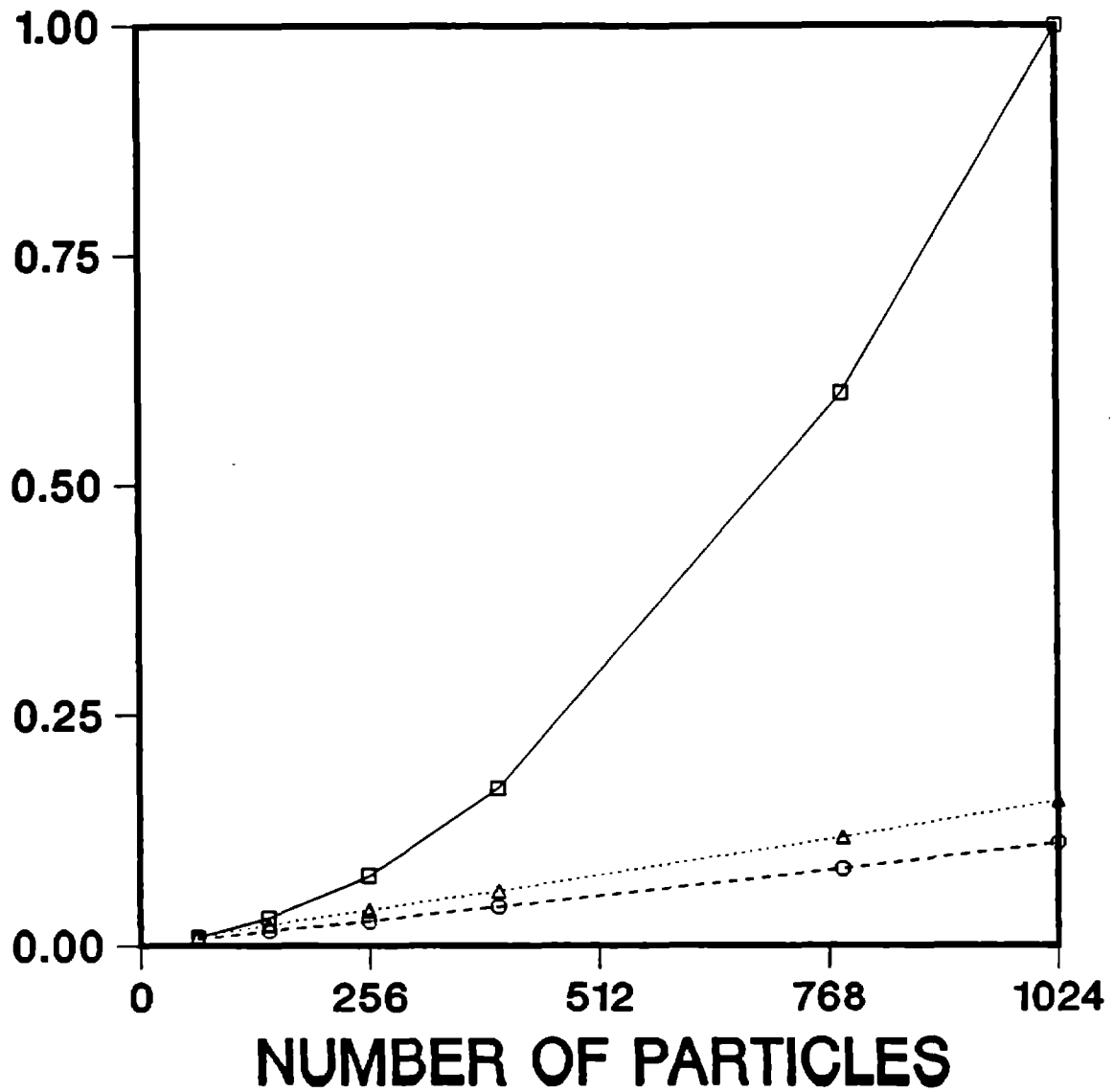


Fig. 3. Normalized cpu time for the BUCKSHOT code for two species vs. the number of particles per species per slice. The solid line is for the direct summation solver, the dashed line is for the new solver with $M = 2$ and the dotted line is for $M = 4$.

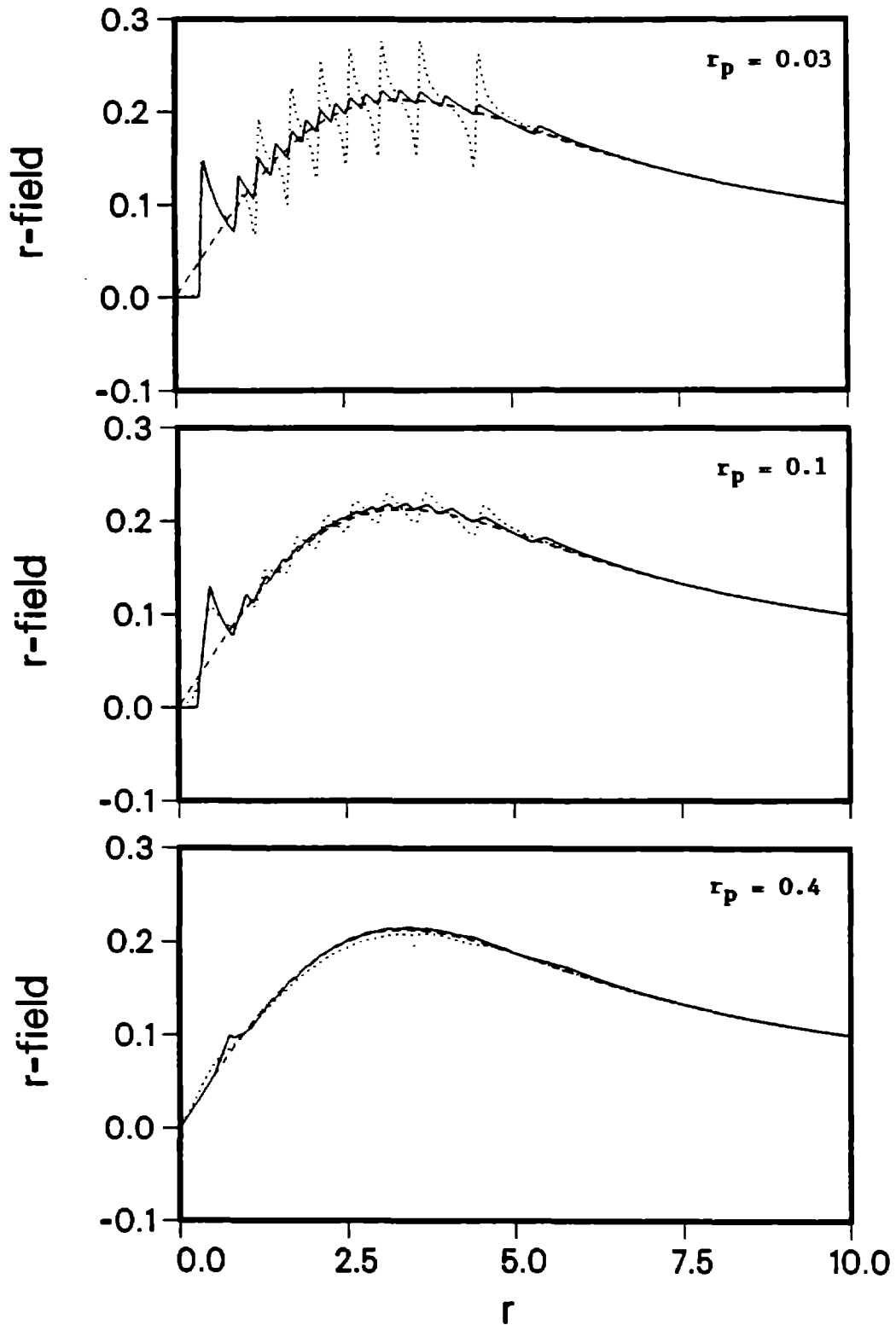


Fig. 4. Comparing fields from direct summation and new solvers with exact Gaussian field for different simulation particle sizes. Solid line is for new solver ($M = 2$), dashed is for exact Gaussian and dotted is for the direct summation solver. $N = 256$ $a = 3.0$

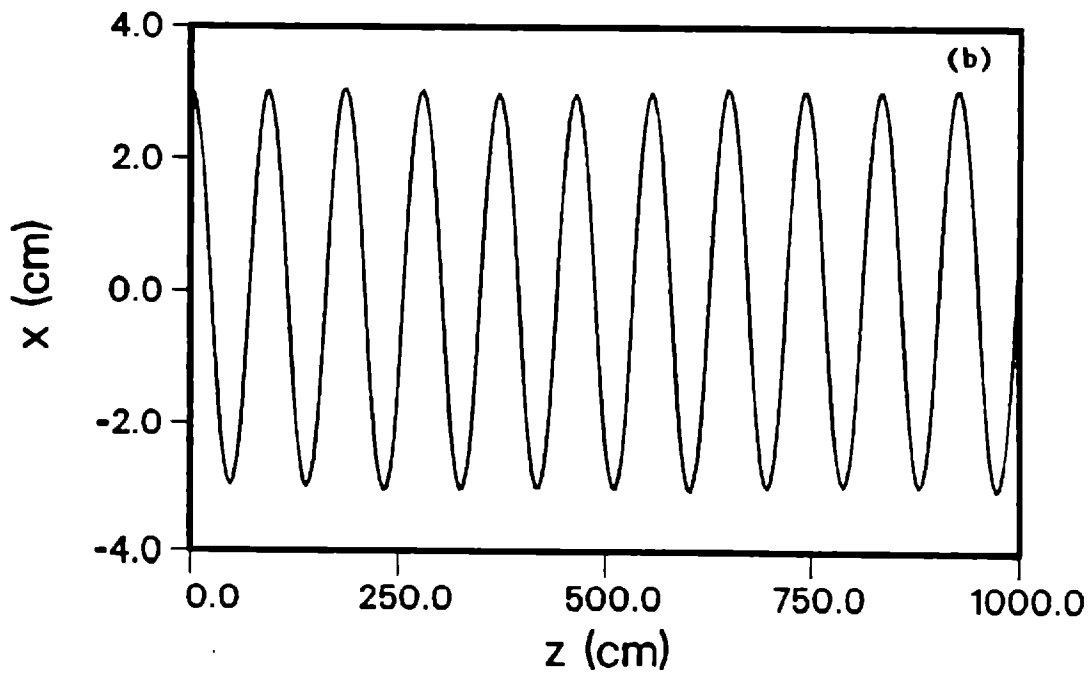
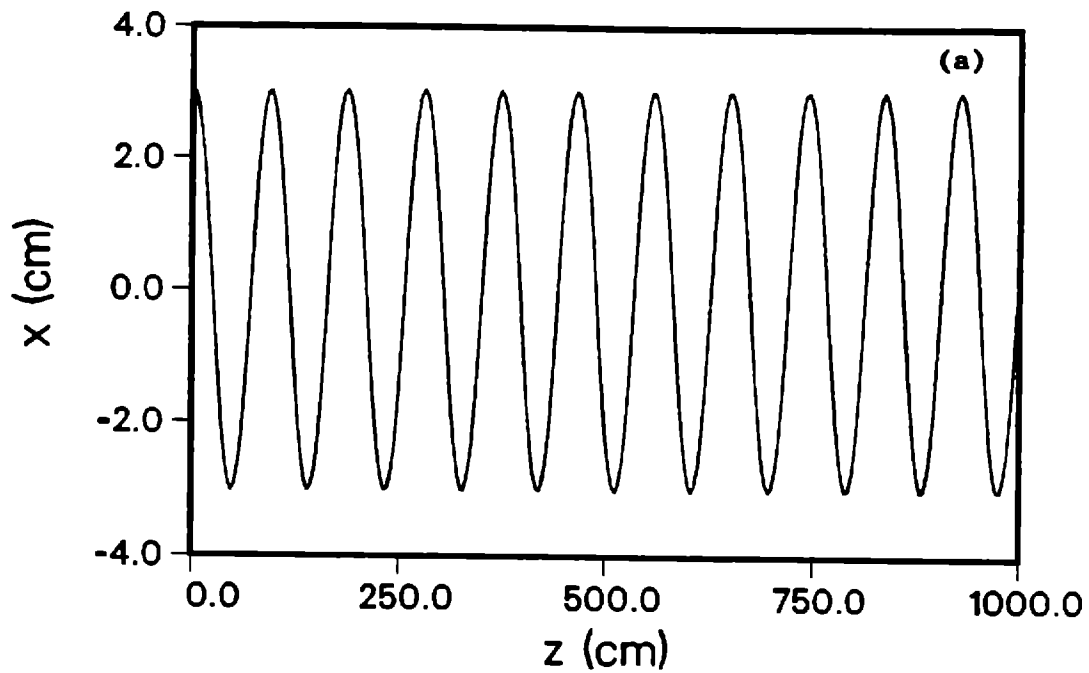


Fig. 5. Single particle orbit in a Gaussian charge distribution.
 Parameters: $I = 1$ kA, $\gamma = 2$, $a = 3$ cm, $x_0 = 3$ cm and $v_0 = 0$.
 (a) Exact Gaussian with step size $dz = 4.0$ cm.
 (b) New solver ($M = 2$), $N = 256$, $r_p = 0.4$ cm, $dz = 4.0$ cm.

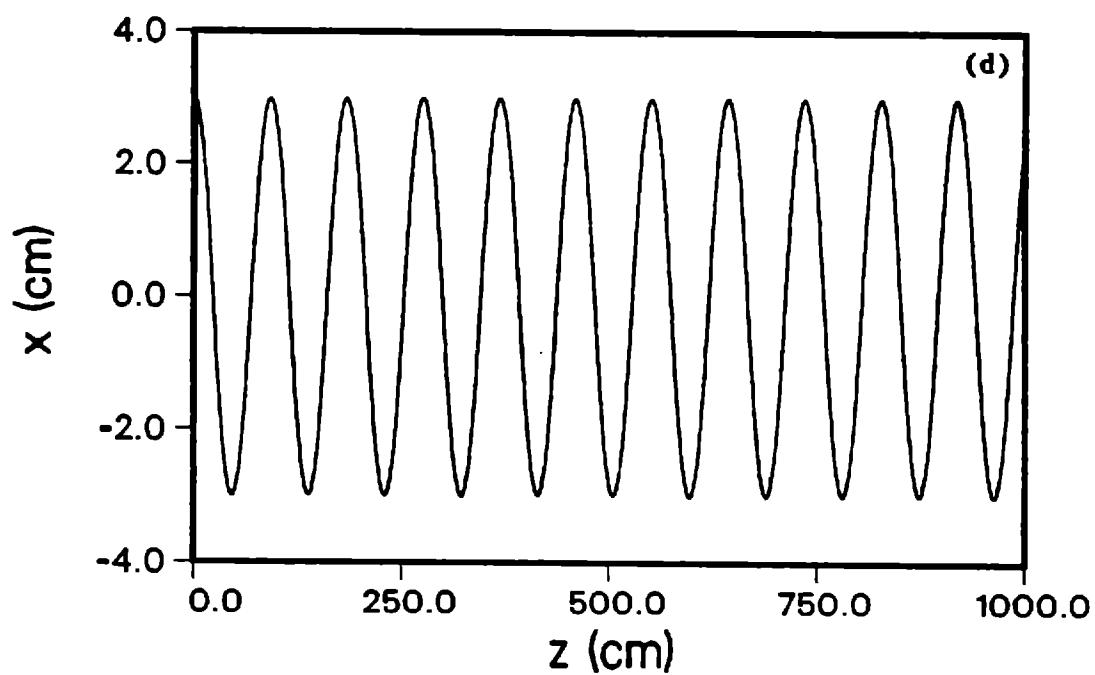
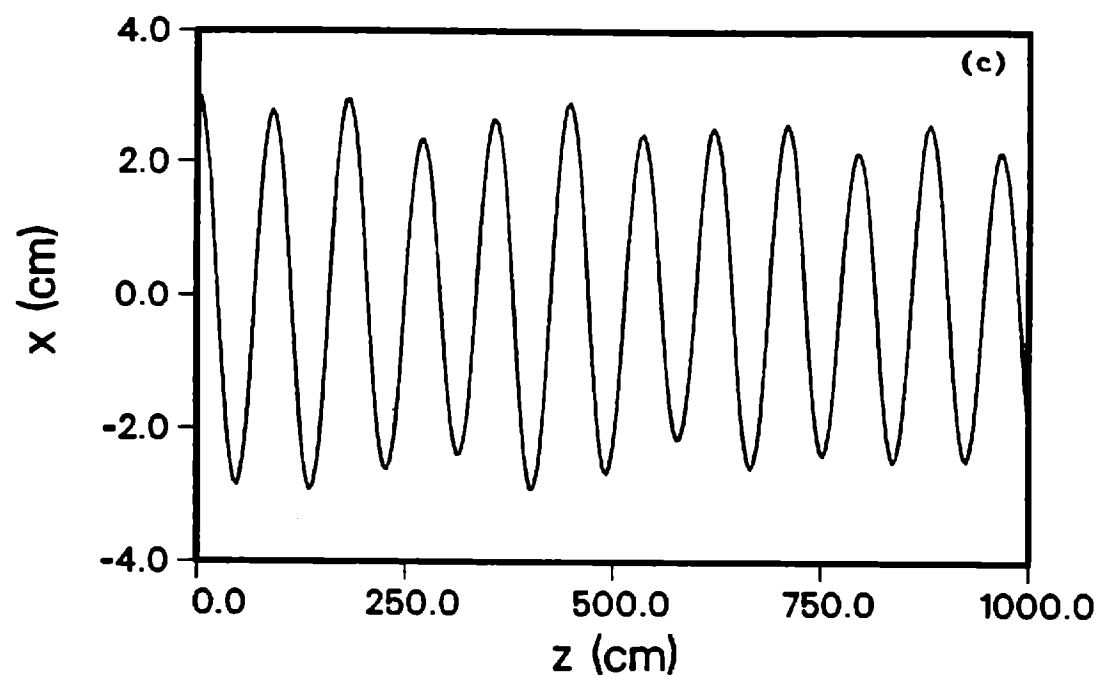


Fig. 5. Single particle orbit in a Gaussian charge distribution.
 (c) New solver ($M = 2$), $N = 256$, $r_p = 0.1$ cm, $dz = 4.0$ cm.
 (d) New solver ($M = 2$), $N = 256$, $r_p = 0.1$ cm, $dz = 1.0$ cm.

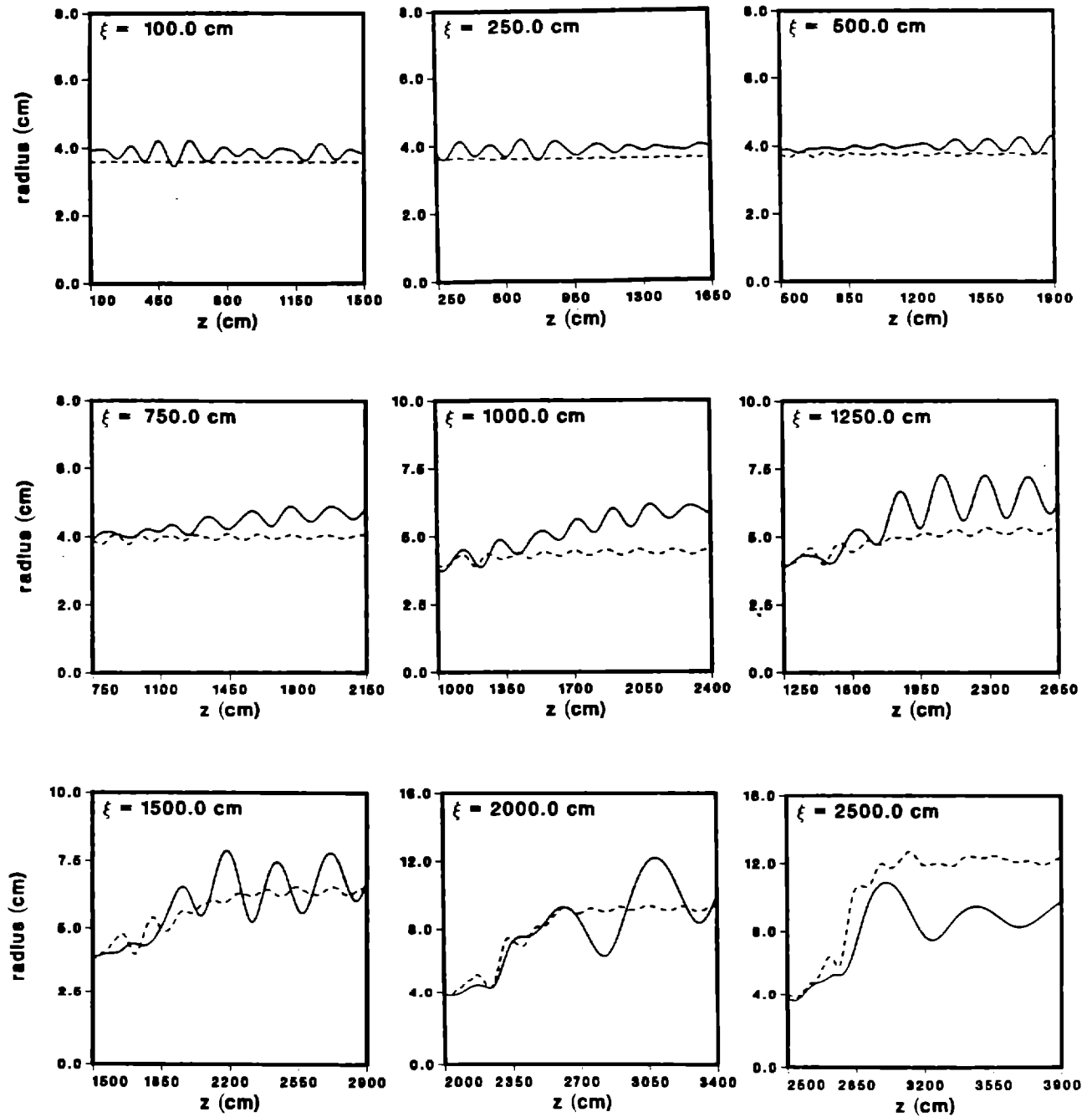


Fig. 6. Slice history of beam (solid) and ion (dashed) RMS radius for different slices using direct summation solver. Simulation parameters: $r_b = 4.0$ cm, $r_i = 3.7$ cm, $x_b = 0.3$ cm, $y_b = 0.2$ cm, $I_b = 0.7$ kA, $\gamma = 5.9$, $B_z = 30.0$ Gauss, $f = 1.0$, $r_p = 0.6$ cm, $dz = 5.0$ cm and $N_b = N_i = 256$.

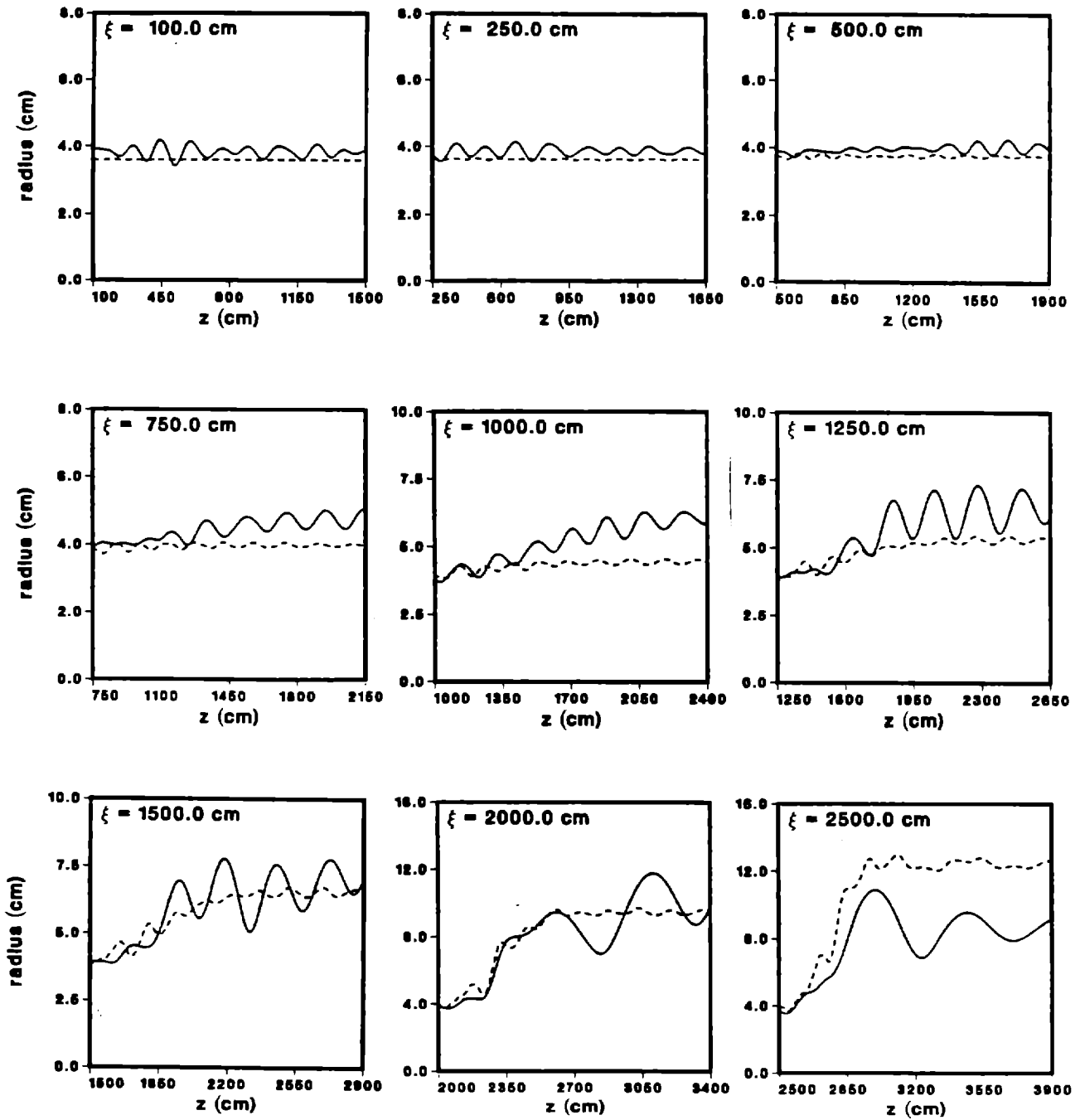


Fig. 7. Slice history of beam (solid) and ion (dashed) RMS radius for different slices using new solver with $M = 2$. Same parameters as Fig. 6.

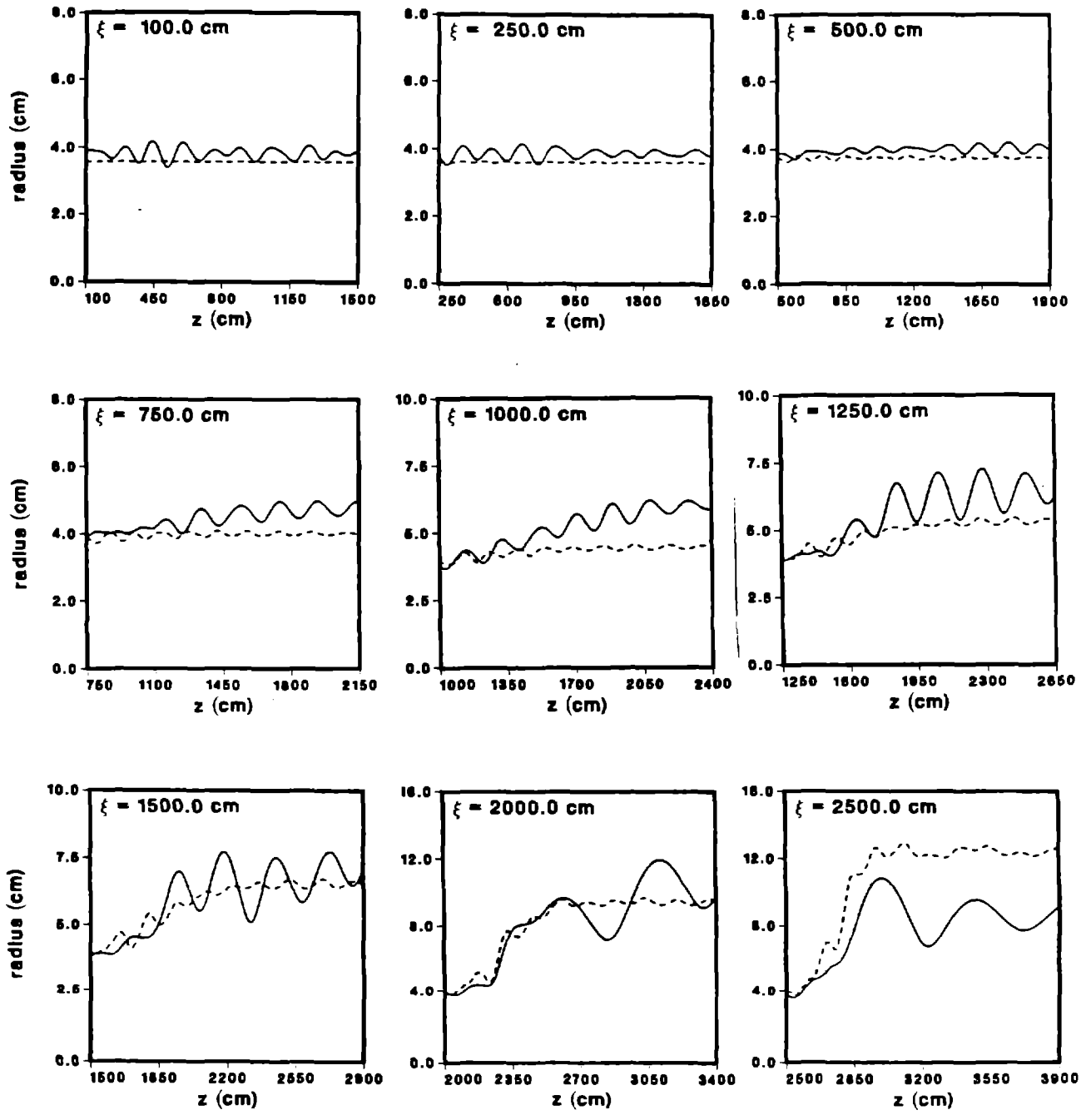


Fig. 8. Slice history of beam (solid) and ion (dashed) RMS radius for different slices using new solver with $M = 4$. Same parameters as Fig. 6.

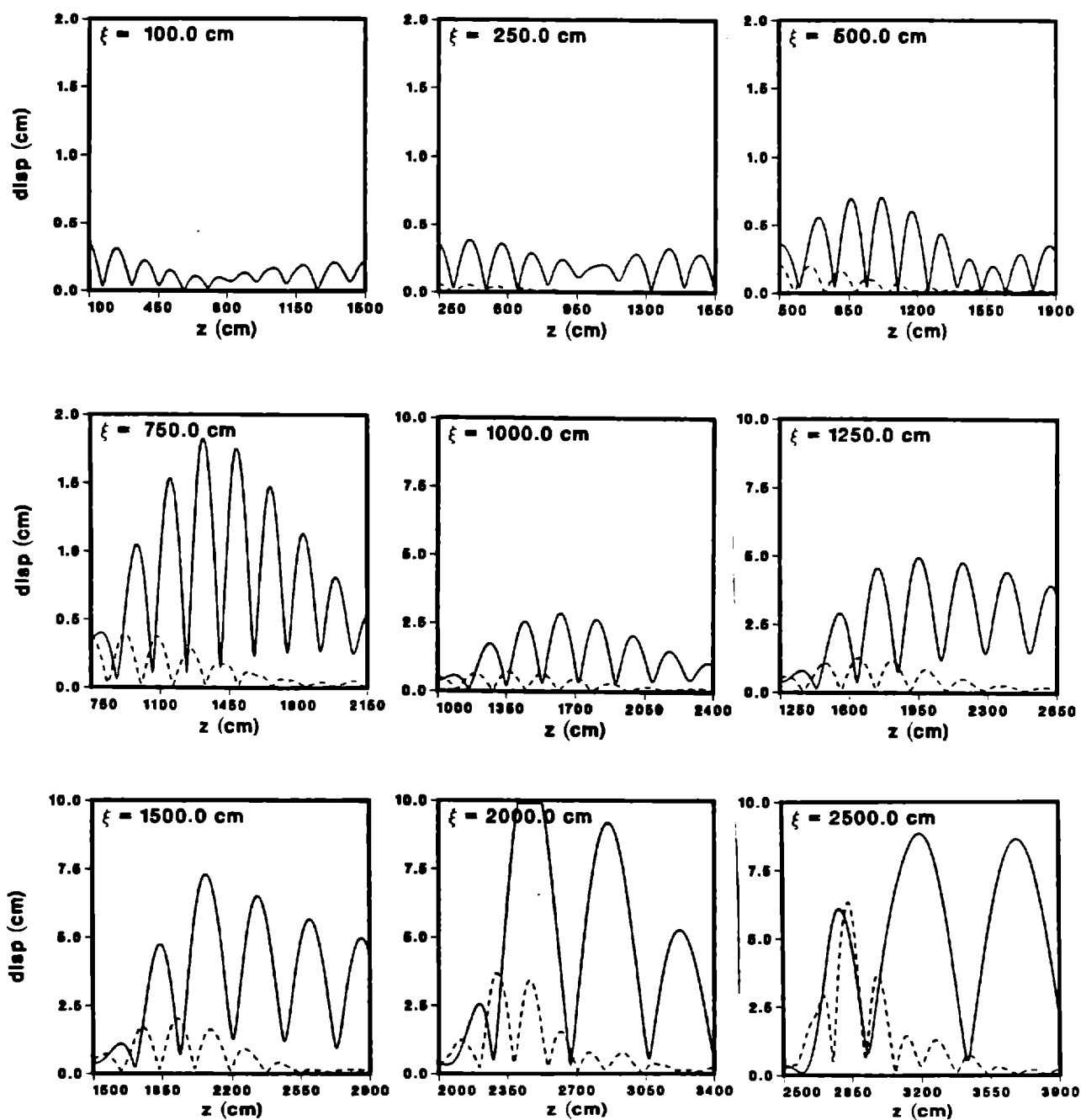


Fig. 9. Slice history of beam (solid) and ion (dashed) displacements for different slices using direct summation solver. Same parameters as Fig. 6.

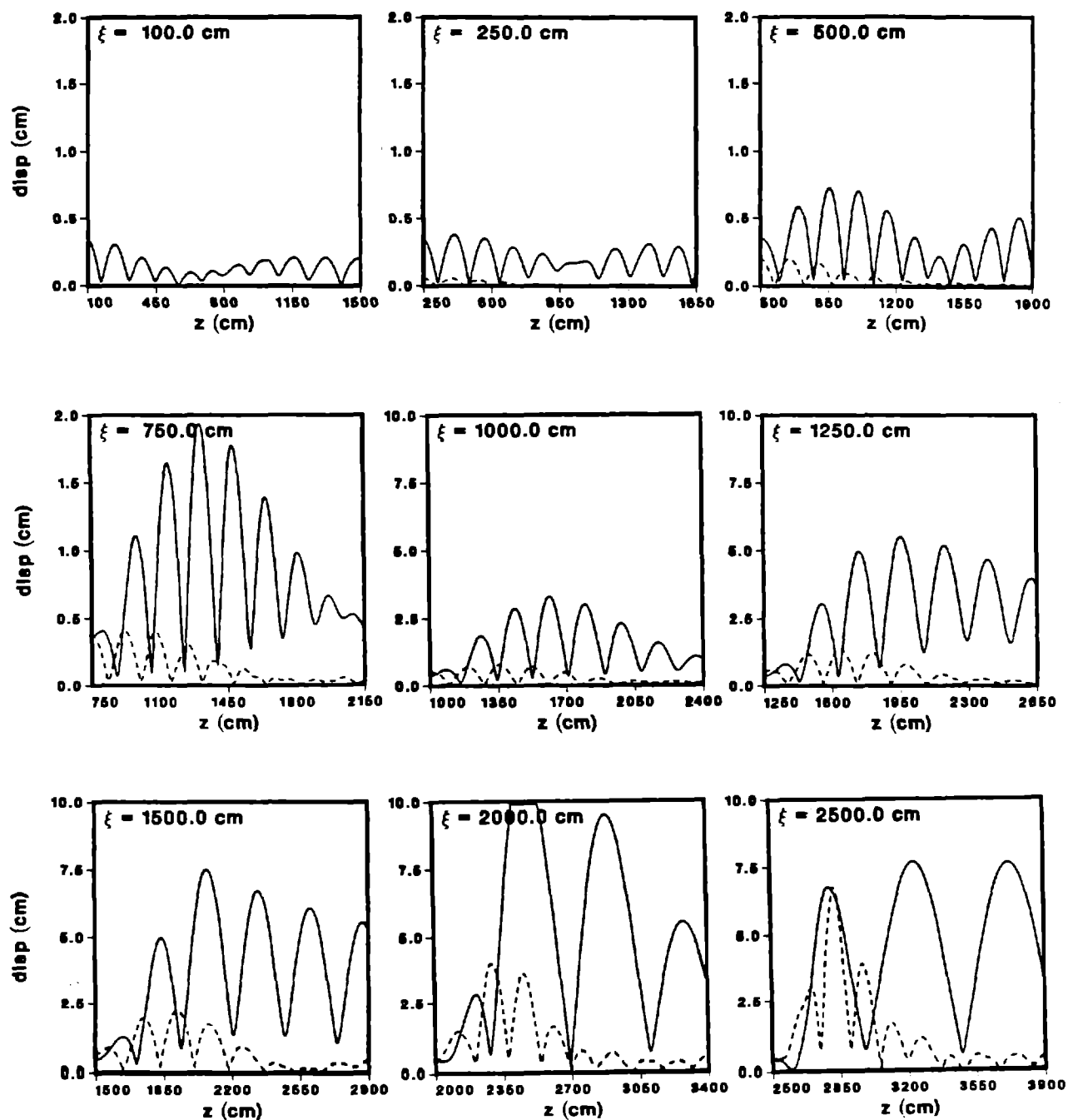


Fig. 10. Slice history of beam (solid) and ion (dashed) displacements for different slices using new solver with $M = 2$. Same parameters as Fig. 6.

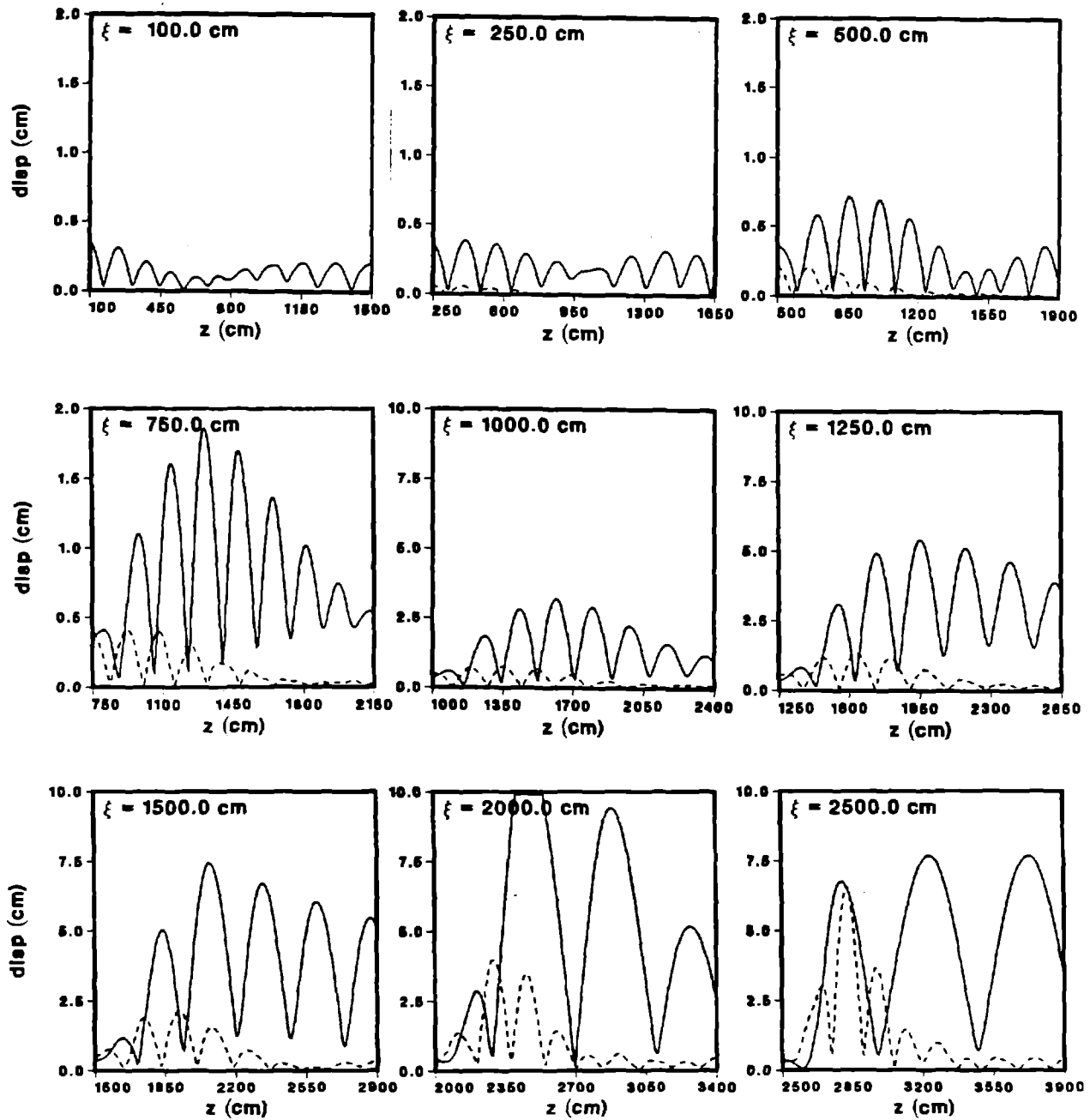


Fig. 11. Slice history of beam (solid) and ion (dashed) displacements for different slices using new solver with $M = 4$. Same parameters as Fig. 6.

DISTRIBUTION:

Unlimited Release

Air Force Weapons Laboratory
Kirtland Air Force Base
Albuquerque, NM 87117
Attn: Dr. B. B. Godfrey

Defense Advanced Research Projects Agency
1400 Wilson Blvd.
Arlington, VA 22209
Attn: H. L. Buchanan
B. Hui

Lawrence Livermore National Laboratory
P. O. Box 808
Livermore, CA 94550
Attn: Simon Yu

Los Alamos National Laboratory
University of California
P.O. Box 1663
Los Alamos, NM 87544
Attn: H. O. Dogliani, H818
J. Mack, P940
T. P. Starke, P942

Mission Research Corporation
1720 Randolph Road, SE
Albuquerque, NM 87106
Attn: D. Welch
T. Hughes
M. Mostrom
K. Struve

Mission Research Corporation
8560 Cinderbed Road-Suite 700
Newington, VA 22122
Attn: Khanh Nguyen

Naval Research Laboratory
Department of the Navy
Washington, D. C. 20375
Attn: M. Lampe
R. Hubbard
G. Joyce
J. Krall
S. Slinker
R. Fernsler

Naval Surface Weapons Center
White Oak Laboratory
Silver Spring, MD 20910
Attn: Eugene E. Nolting (H23)
Han Uhm

Pulse Sciences, Inc.
600 McCormick Street
San Leandro, CA 94577-1110
Attn: S. D. Putnam

SSC Lab
2550 Beckeymead Avenue
Mail Stop 1046
Dallas, TX 75237
Attn: Gordon Leifeste

Science Applications Int'l Corp.
5150 El Camino Real, Suite B-31
Los Altos, CA 94022
Attn: L. Feinstein

Science Applications Int'l Corp.
1710 Goodridge Drive
McLean, VA 22102
Attn: W. Reinstra

Southwest Research Institute
Drawer 28510
6220 Culebra Road
San Antonio, TX 78284
Attn: C. S. Lin

Commander
Space & Naval Warfare Systems Command
PMW-145
Washington, DC 20363
Attn: Lt. Bill Fritchie

Titan Technologies-Spectron Division
2017 Yale Blvd., SE
Albuquerque, NM 87106
Attn: R. B. Miller
J. Smith

University of Alaska
Geophysical Institute
Fairbanks, AK 99701
Attn: S. I. Akasofu
L. C. Lee

University of Texas at Austin
Institute for Fusion Studies
Austin, TX 78712
Attn: T. Tajima

Internal Distribution:

1000 V. Narayanamurti
1200 J. P. VanDevender
1201 M. J. Clauser
1230 J. J. Ramirez
1231 J. R. Lee
1240 K. R. Prestwich
1241 J. R. Freeman
1241 R. W. Lemke
1241 B. M. Marder
1241 K. J. O'Brien
1241 C. L. Olson
1241 J. W. Poukey
1241 D. B. Seidel
1241 I. R. Shokair (15)
1241 J. S. Wagner (15)
1242 B. N. Turman
1242 C. A. Frost
1242 R. J. Lipinski
1242 M. G. Mazarakis
1242 S. L. Shope
1244 J. M. Hoffman
1260 D. L. Cook
1265 J. P. Quintenz
1270 J. K. Rice
1275 R. A. Gerber
3141 S. A. Landenberger (5)
3151 W. I. Klein (3)
3141-1 C. L. Ward for DOE/OSTI (8)
8524 J. A. Wackerly

